Fusion Engineering and Design 222 (2026) 115408

Contents lists available at ScienceDirect

Fusion Engineering and Design

journal homepage: www.elsevier.com/locate/fusengdes

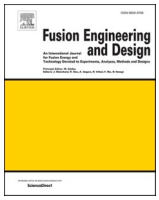

A shinethrough detector and interlock for neutral beam injection operations on MAST-U

Roy McAdams *, Philippe Jacquet, Ian Day, Effy Rose, Andrew Ash, Jake Ashton, Hana El-Haroun, Paul Jepson, David Keeling, Damian King, Robert King, Stephen Marsden, Alistair McShee, Maria Nicassio, Dean Payne, Robert Proudfoot, Ridhima Sharma, Jamie Smith, Christopher Tame, Thomas Wilson

UKAEA (United Kingdom Atomic Energy Authority), Culham Campus, Abingdon, Oxfordshire OX14 3DB, United Kingdom

ARTICLE INFO

Keywords:
Neutral beam injection
Shinethrough protection
MAST-U

ABSTRACT

Neutral Beam Injection (NBI) is a powerful tool and is very commonly used for heating, current drive and diagnostics on magnetically confined devices for fusion power development. Not all the neutral beam power is deposited within the plasma. This shinethrough power must be dealt with at the first wall and any components irradiated by it must be protected against excessive heating. This paper describes the design, implementation and testing of a shinethrough detector and interlock for the MAST-U machine. It is based on the detection of the infrared emission from the beam dump which can then be used to terminate the beam pulse if this exceeds a required threshold. The effects on the detected signal of loosely bound material ("dust") on the beam dump is also discussed.

1. Introduction

Neutral Beam Injection (NBI) is used on almost all magnetically confined fusion plasma research devices. Its purposes are to heat the plasma, drive current and for diagnostic measurements. The beam energy is generally selected (especially for heating and current drive) to deposit the beam power near the centre of the plasma. This means, in practice, that not all the beam power is absorbed by the plasma and the fraction remaining after leaving the plasma is referred to as the beam shinethrough fraction. Neutral beams have high power and high power density and the shinethrough is capable of damaging components if the plasma density is too low or there is a sudden loss of plasma such as a disruption. Components irradiated by shinethrough must be protected against excessive heat loading and subsequent damage.

As an example, the Joint European Torus (JET) had sixteen deuterium positive ion based neutral beam injectors each capable of 2 MW of neutral beam power at 125 keV energy, arranged in two injection boxes [1]. A multi-layer approach was taken to shinethrough protection on JET [2,3] of which a hardwired interlock based on detection of plasma produced bremsstrahlung was the main protection. This was backed up by two Plant Enabled Window Systems (PEWS1 and PEWS2). PEWS1 used a real time measurement of the plasma density which had to be high enough for the beam voltage and pulse duration for injection to proceed or continue. PEWS2 was a real time calculation of the bulk and surface temperatures of the Plasma Facing Components (PFCs) intercepted by the shinethrough, based on simple models of beam absorption and thermal response of PFCs subjected to shinethrough loads. If particular temperatures, based on the properties of the components, were exceeded then the injectors were switched off.

The Mega-Ampere Spherical Tokamak - Upgrade (MAST-U) [4] presently has two deuterium positive ion based neutral beam injectors. An additional Double Beam Box (DBB) injector is currently under construction. The present injectors are each capable of 75 keV, 65 A beam extraction, giving up to 2.5 MW each of neutral beam power with pulse lengths up to 1 s [5,6]. The only shinethrough protection previously available in MAST was a plasma current interlock which indicated the presence or absence of plasma current. As the experimental campaigns move towards longer pulse lengths, the potential for overheating and damage is much greater and particularly for fault scenarios with very low plasma density. A new shinethrough detector and interlock adequate for the enhanced MAST-U NBI performances and plasma scenarios was therefore required.

* Corresponding author.
E-mail address: roy.mcadams@ukaea.uk (R. McAdams).

https://doi.org/10.1016/j.fusengdes.2025.115408
Received 8 July 2025; Received in revised form 12 August 2025; Accepted 25 August 2025
Available online 5 September 2025

This paper describes the design, implementation and testing of the shinethrough detector and interlock for MAST-U. It is used for the present beamlines and will also be used for the new Double Beam Box under construction.

2. Shinethrough on MAST-U

2.1. NBI arrangement and the beam dumps

The arrangement of the two NBIs currently used on MAST-U is shown in Fig. 1(a). These are designated South (SS) and South West (SW). The SS injector is on the equatorial plane of the machine with a tangency radius of 70.5 cm to provide on-axis heating. The SW injector has a tangency radius of 80 cm and is raised by 65 cm from the equatorial plane to provide plasma heating and off-axis current drive.

The beam dumps absorb any shinethrough from the beams and protect the vessel wall. These must not be damaged and should be, in turn, protected by the shinethrough interlock. The beam dumps consist of eight Carbon Fibre Composite (CFC) tiles in the central region and are surrounded by sixteen graphite tiles.

The thermal conductivity of the CFC tiles is significantly higher along the beam axis direction and the vertical direction orthogonal to the equatorial plane than in the horizontal direction. This allows the heat from the beam to be spread out rapidly and minimize local heating, higher temperatures and thermal gradients. The shinethrough detector, described in Sections 3 and 4, monitors the heating of the central region of the beam dump. Fig. 1(b) shows a view of the MAST-U vessel interior and indicates the SS beam dump.

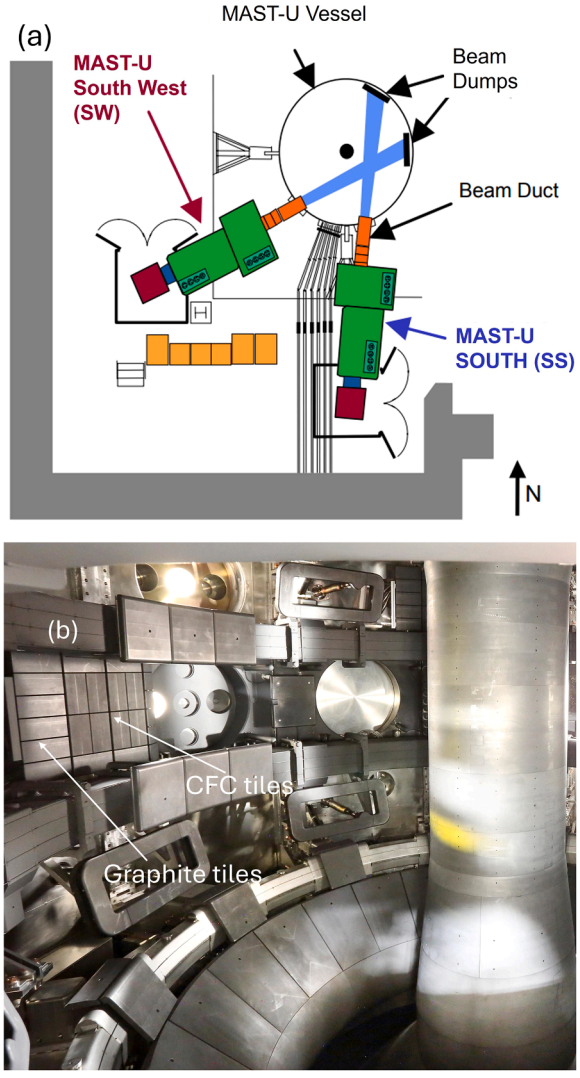

Fig. 1. (a) The arrangement of the neutral beam injectors on MAST-U. (b) The interior of the MAST-U vessel showing the South (SS) beam dump.

2.2. Shinethrough power estimate and tile heating

The shinethrough fraction is the fraction of injected neutral beam power that emerges from the plasma and strikes the dumps. The on-axis and off-axis shinethrough fraction at 75 keV beam energy has been calculated for a typical plasma scenario for MAST-U. Fig. 2 shows the shinethrough fraction against a scan of the integrated plasma density along the line of sight of the MAST-U interferometer used to measure it.

As expected, the shinethrough fraction is higher for the off-axis beam by a few percent because the actual plasma density along the off-axis SW beam path will be lower than that for the on-axis SS beam.

The beam profile at the beam dump, in the absence of a plasma, has been calculated for a high power 75 kV, 60 A beam with 2 MW of neutral beam power using the PINI Simulator code [7]. The results are shown in Fig. 3 where the white contour is the $1/e \times$ peak power density contour. The peak power density is ~50 MWm^{-2}. The shinethrough diagnostics will view an area of a approximately 20 cm^2 of the dump central region and so the average peak power density over this area will be a little lower than 50 MWm^{-2}.

In Fig. 4 the surface temperature of a CFC tile has been calculated for incident power densities of 20, 30, 40 and 50 MWm^{-2}. The temperatures have been calculated with a 1D heat transfer model.

Damage to the CFC tiles could occur at temperature of 1400 °C or above. In practice, a more conservative limit of ~700 °C will be used. From Fig. 4 the maximum allowable temperature would be reached after 0.35 s for 40 MWm^{-2} incident power density and the rate of temperature rise is ~4000 °C/s. Any interlock based on shinethrough detection must then operate on a timescale of much less than 0.1 s to limit the tile temperature. It must also be noted that the plots in Fig. 4 start at 0 °C. Radiation is the main cooling mechanism for the tile and the starting temperature can ratchet up particularly with relatively frequent pulsing through a day of operation. In principle if very low density plasmas are run frequently this could limit the beam pulse length. This situation has not yet been encountered.

An infra-red (IR) view of the SW beam dump during pulse 48444 is shown in Fig. 5. This is a beam into vacuum pulse (no plasma present) with a power of 1.6 MW and a duration of 140 ms. The peak temperature is ~455 °C. The temperature scale in the picture assumes an emissivity and window transmission of unity. The peak power density is calculated as ~36 MWm^{-2} using PINI Simulator and then using the 1D heat flow model this leads to an estimated maximum temperature of ~ 670 °C. The

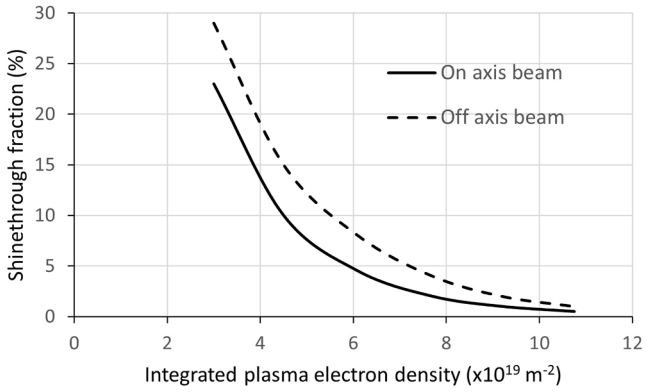

Fig. 2. The shinethrough fractions for both the on-axis and off-axis beamlines at 75 keV plotted against the integrated plasma density along the interferometer line of sight in the midplane.

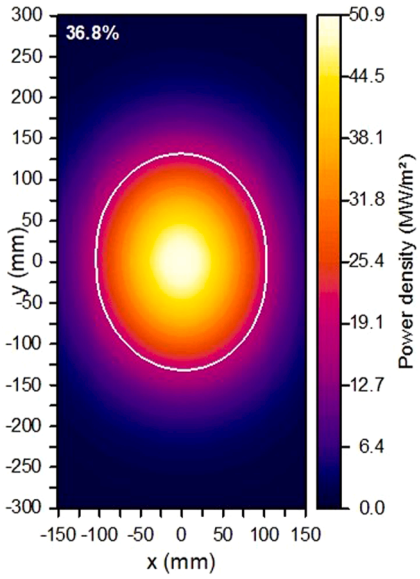

Fig. 3. The beam profile, in the absence of a plasma, for a 75 kV, 60 A beam with 2 MW of neutral beam power. The contour is 1/e x peak power density or 36.8 %.

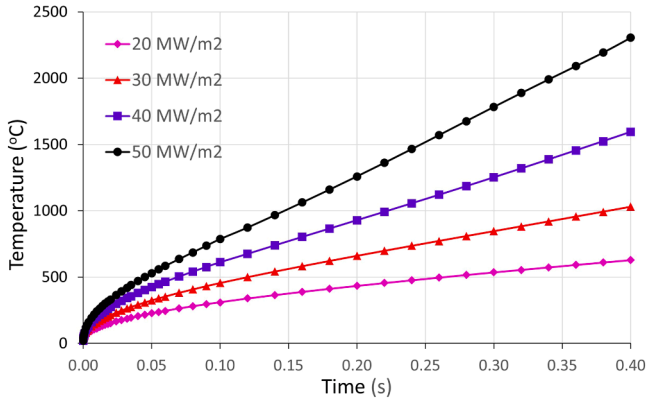

Fig. 4. The calculated surface temperature of a CFC tile with applied heat fluxes of 20, 30, 40 and 50 MWm^{-2}.

difference in the two temperatures can be explained by the calibration of the temperature through the emissivity and transmission. This is further described in Section 5.3.

3. Overall concept of the detector and interlock

The aim of the shinethrough detector and interlock is to monitor the heating of the beam dump tiles by the neutral beam. If the signal, representing the tile temperature, exceeds a pre-set threshold then the NBI control system should act immediately to switch off the beam. The overall concept for the system is shown in Fig. 6.

IR emission from the beam dump passes through a MAST-U port equipped with a sapphire window into the detector optical system. A gate valve is used: it is open during NBI pulses but closed during MAST-U cleaning discharges. This shutter is also used in conjunction with a test lamp to check that the system is operational: light from the test lamp is reflected from the shutter and can be detected by the system. A long pass filter (λ>1350 nm) is used to filter out IR emission from the plasma edge. The resulting IR emission is then collected and focussed into 30 m of optical fibre to where the detector is housed, outside the MAST-U blockhouse. This is necessary so that the magnetic fields of the

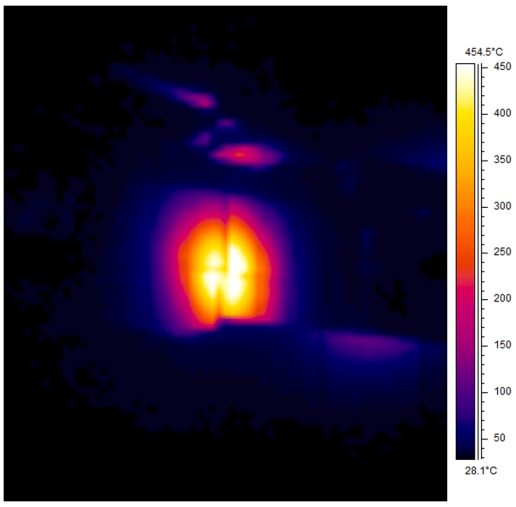

Fig. 5. Infra-red view of the SW beam dump during a 1.6 MW 140 ms beam into vacuum pulse (MAST-U pulse 48444). The temperature scale is not calibrated (see text).

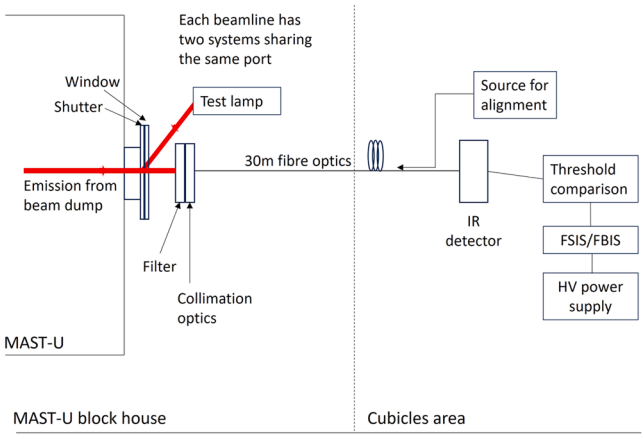

Fig. 6. The overall concept of the shinethrough detector and interlock.

tokamak do not influence the detector performance (as was found in an earlier version of the system), and to avoid potential damage to the electronics from the high energy neutrons produced by the deuterium-deuterium nuclear reactions in MAST-U. The filter and collection optics have an adjustable mount which, in combination with a suitable LED light source that can be coupled into the fibre optics, allows the system to be aligned.

The IR optical collection and detection system was simulated using the Zemax software [8]. In particular, the choice of the IR wavelength to be detected, collection optics, fiber-optics and detector was a compromise between IR emission power density versus wavelength and wavelength response of the optical components in the system. Many different options were considered to optimize performance based on expected emission behaviour and available components.

The signal from the IR detectors is compared with a pre-set threshold. The result of the threshold comparison is an input to the Fast Safety Interlock System (FSIS). FSIS cycles on a 100 μs period looking at the input from the threshold comparison. If the threshold is exceeded, by either detector, for a preset cycle count of 100 (10 ms) then a signal is sent to the Fast Beam Interlock System (FBIS), the overall fast interlock management system for the beam. FBIS consists of a 1 kHz pulse train indicating a safe operational state. The signal from FSIS interrupts this pulse train. Interruption of this pulse train causes the HV supply in that beamline to switch off. Note that FBIS also looks at other

inputs such as the bend magnet current for removal of residual ions in the beamline, the status of the neutraliser gas valve and the duct pressure among others.

4. Design and laboratory testing of the shinethrough detector

4.1. Choice of spectral range

The aim of the detector is to measure the infra-red emission of the beam dump tiles due to heating by beam impingement. In almost all cases this will be in the presence of the MAST-U plasma. Thus, it is important to select the wavelength range to be detected carefully so that the plasma emission does not affect the measurement. Fig. 7 shows a spectral survey in the near infra-red of the emission from the MAST-U plasma in the divertor region

Since no emission is recorded in the region above 1350 nm it was decided to detect radiation in this region to ensure only radiation from the beam dump is measured.

4.2. System design

The design and optimization of the system was carried out using the Zemax software package. The system was modelled as shown in Fig. 6 from source to detector output with a blackbody source at the correct distance of 4 m from the filter simulating the beam dump. The source dimensions were 180 × 180 mm with an emissivity of 0.9. Various options for the individual components were considered and the final choices are described here.

An IR detector in combination with an edge long pass filter was chosen to select and detect the radiation from the beam dump. The detector is a Thorlabs PDA30B Ge detector with the advantage of a switchable gain. The longpass filter is a Thorlabs FEL1350 filter with a cut-on wavelength of 1350 nm. The transmission of the filter is zero at wavelengths <1350 nm and 80 % at wavelengths between 1350 and 2200 nm.

The transmission of the 30 m optical fibre also plays a role both in determining the wavelength reaching the detector but also in overall transmission of the system. A 0.39NA (numerical aperture) 400 μm fibre was chosen. Although the transmission of this fibre falls at wavelengths above 1600 nm compared to a lower NA fibre with higher transmission, this is compensated in signal terms by the larger numerical aperture. A Thorlabs F810FC-1550 collimator was used to focus beam dump emission into the fibre. FC connectors are used to attach the fibre to the collimator and detector.

Fig. 8 shows the transmission of the filter, 30 m of optical fibre and the responsivity of the detector, all obtained from digitization of the manufacturer's data. A total responsivity is also shown, which is obtained by multiplying the above together although this ignores coupling and connector efficiencies and collimator transmission which is <0.4 % reflectivity between 1350 and 1625 nm. It shows that the STI optical system is responsive to wavelengths in the region 1350–1700 nm. The window is made of sapphire and has a transmission of ~85–86 % over the responsive wavelength range.

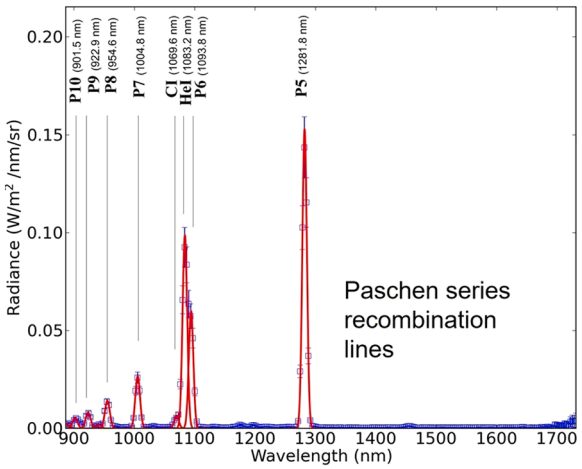

Fig. 7. Spectral survey of the near infra-red emission of the MAST-U plasma in the divertor region.

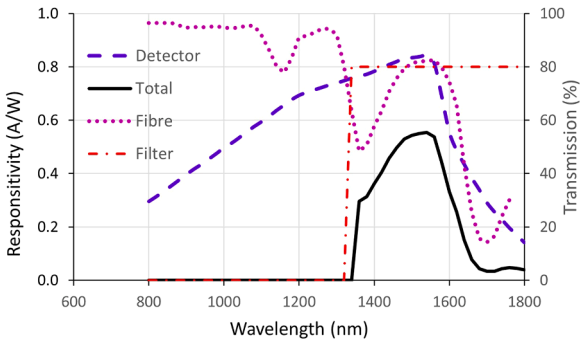

Fig. 8. Transmission of the filter and 30 m of the optical fibre together with the responsivity of the detector.

An exploded view of the optical head components is shown in Fig. 9 showing how the components fit together.

4.3. Bench testing of the system

The basic system was bench tested to ensure that the signal levels and overall response with source temperature were behaving in accordance with the Zemax modelling of the system. The arrangement used is shown in Fig. 10.

A blackbody source was used to simulate the beam dump and this was placed at the same distance (~4 m) from the optical head as the beam dump on MAST-U. The blackbody source had a diameter of 3 cm.

In Fig. 11 the measured output signal from the system is plotted against the blackbody source temperature at two different gains of 30 dB and 40 dB on the detector. Also plotted are the results of the Zemax simulation of the complete system to be used on MAST-U assuming a 30 dB gain. The figure shows that the measured signals have the same general trend as the simulation.

The difference between the results of the simulation of the system to be deployed on MAST-U and those from the system tested on the bench is due to a number of factors. The testing was carried out without a sapphire window whereas there is one on MAST-U. The implemented system has a fibre of 30 m length whereas the bench tests used a 5 m length fibre. The longer fibre has between 70–85 % of the transmission of the 5 m fibre in the wavelength range 1400–1600 nm. In addition, back illumination of the blackbody showed that the area viewed had a diameter of ~5 cm. This is wider than the blackbody (3 cm diameter) itself and some of the cooler regions of the blackbody housing would also have been viewed by the detector.

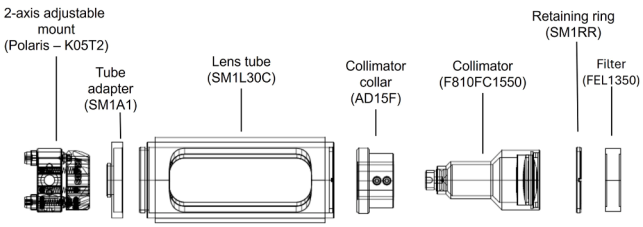

Fig. 9. An exploded view of the optical head components. Thorlabs Inc. component part numbers are indicated.

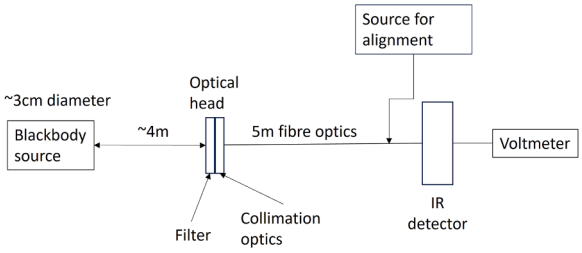

Fig. 10. Bench testing arrangement of the detector.

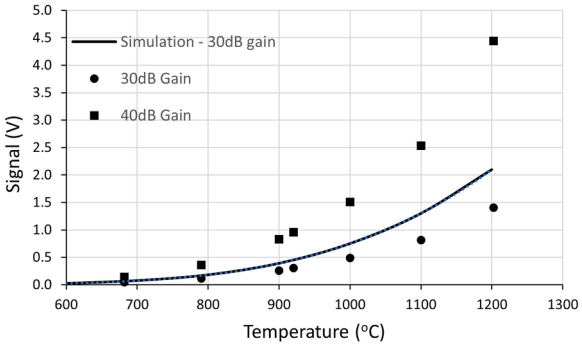

Fig. 11. The results of bench testing the detector and comparison with the simulation of the MAST-U system.

5. System commissioning and operation

5.1. Implementation, commissioning and operation

In Fig. 12, a photograph of the system in place on MAST-U is shown.

The four detectors (two on each beamline for redundancy) were commissioned by running beam into vacuum pulses to allow the beam dump to receive beam power and heat up. The threshold for Shinethrough Interlock (STI) operation was set low initially to ensure that the system tripped the beam. As an example, the testing of one of the SW beamline detectors is shown in Fig. 13 for MAST-U pulse 48445. The beam voltage and current are 65 kV, 47 A (1.6 MW neutral power) and the beam duration is set at 140 ms. The detector gain was set at 60 dB and the trip threshold at 0.5 V.

The upper graph in Fig. 13 shows the accelerator voltage and current, the middle graph shows the output of the two STI detectors and the lower graph shows the FBIS logic state. The greyed area shows the preset beam on period which in this case was 140 ms, although the whole 140 ms is not shown in the plot. The threshold of 0.5 V is exceeded within a few ms of the beam switching on. After the threshold being exceeded for 100 cycles (10 ms) of FSIS, the interlock voltage changes, the FBIS pulse

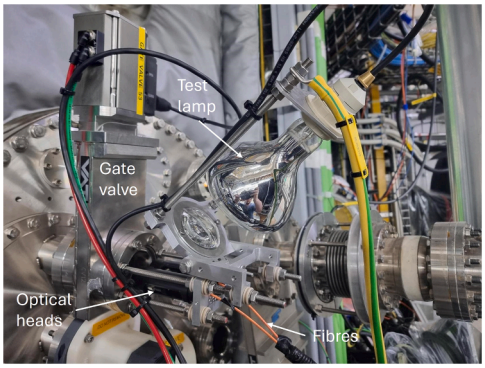

Fig. 12. The optical head system installed on MAST-U.

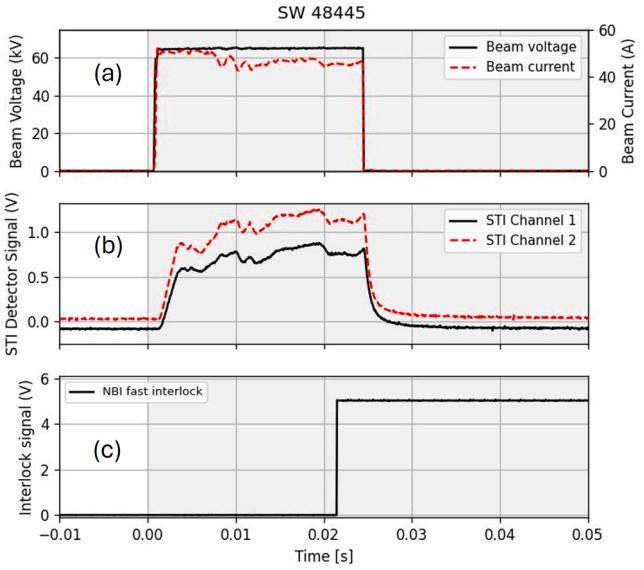

Fig. 13. Commissioning of an STI on the SW beamline – MAST-U pulse 48445. (a) Beam voltage and beam current. (b) ST1 output voltages. (c) NBI fast interlock voltage. The greyed area shows the preset beam on period (140 ms – not all shown).

train is stopped and a signal is sent to switch off the HV power supply to the accelerator and halt the beam operation. The overall time between the threshold being exceeded and the beam being switched off is ~20 ms.

Another example of commissioning of one STI channel for the SW beamline is shown in Fig. 14 for MAST-U pulse 48438. The beam voltage and current are 55 kV, 37 A (1.2 MW neutral power) and the beam duration is set at 200 ms. The detector gain is set at 60 dB and the trip threshold at 1.0 V for STI channel 1 and 11 V for STI channel 2. The threshold for channel 2 was purposely set high in this commissioning step, to verify the Channel 1 interlock chain. Due to the higher threshold compared with that in Fig. 13, the beam dump is heated to a higher

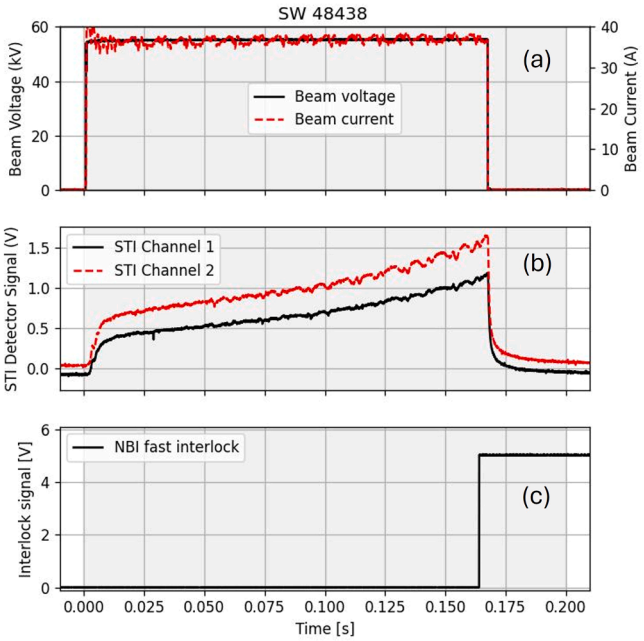

Fig. 14. Commissioning of an STI on the SW beamline – MAST-U pulse 48438. (a) Beam voltage and current. (b) ST1 output voltages. (c) NBI fast interlock voltage. The greyed area shows the preset beam on period (200 ms).

temperature and the STI signal continues to increase during the pulse. When the threshold of 1 V is exceeded, the beam turn-off takes place as expected in a time period of < 20 ms.

Finally, an example of a beam into vacuum pulse is shown in Fig. 15 where the threshold is set high enough such that no trip is expected. For MAST-U pulse 48444 the beam voltage and current are 65 kV, 48 A (1.6 MW neutral power). Both STI detector signals are shown and their threshold and gains were set at 60 dB and 11 V. The set pulse duration was 140 ms. Since the trip threshold is higher than the signal level reached, the beam is not tripped and reaches the preset pulse length.

An example of the use of the STI during an experimental campaign pulse is shown in Fig. 16. It shows the relevant data from pulse 49445 which had a voltage and current of 67.6 kV and 49.9 A (1.72 MW neutral power) on the SW beamline. The SS beamline was also used in this pulse (64.6 kV, 45 A, 1.57 MW). The figure also shows the two STI channel signals, the plasma current and line density as measured on the central axis of the machine together with the plasma current interlock and FSIS interlock signals.

At the start of the pulse for a duration of ~0.1 s the STI signals increased. This is due to shinethrough because the density is low and it even reduces slightly as the beams turn on. The STI signal reduces due to the increase in density through the pulse. At ~ 0.55 s the density fell but not by enough to allow much shinethrough on this off-axis beam. Just before 0.7 s the density fell rapidly along with the plasma current. The Plasma Control System (PCS) issued a signal to turn off the beams due to the plasma current being too low. Before the beam was switched off the STI signals increase until they reached the threshold of 1 V and then the FBIS system state also changed just after the PCS system. The STI signal is constant between 0.2 and 0.55 s as the density is changing. This is a good indication that the detector is not measuring light from the plasma. This was further checked with pulses where the beam failed to fire but the plasma continued. The STI signal did not change in these cases again showing that light from the plasma is not being detected by the instrument. Incidentally, the SS beam came on 0.13 s after SW (as requested) and that beamline STI signals did not show the initial increase and fall as shown on SW. Additionally the SS STI signals did not reach the trip threshold by the end of the beam pulse probably because of the higher on-axis plasma density.

A final example is shown in Fig. 17 where the end of pulse 50524 is shown for the SW beam (66.6 kV, 48.3 A, 1.66 MW of neutral power). In this case the central line density began to fall at ~0.78 s but the plasma current fell slowly. The SW STI detected increasing shinethrough and switches off the beam before the plasma current fell to a low enough value for the Plasma Control System to issue a beam turn off signal.

These two examples of STI operation illustrate how the systems can act to protect the beam dump tiles adding extra protection and redundancy to the plasma current interlock and protecting against low density plasma events.

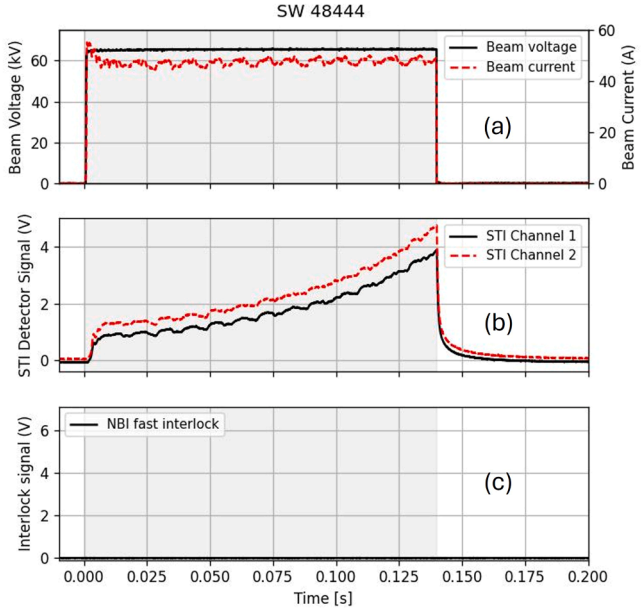

Fig. 15. Commissioning of an STI on the SW beamline – MAST-U pulse 48444. (a) Beam voltage and current. (b) ST1 output voltages. (c) NBI fast interlock voltage. The greyed area shows the preset beam on period (140 ms).

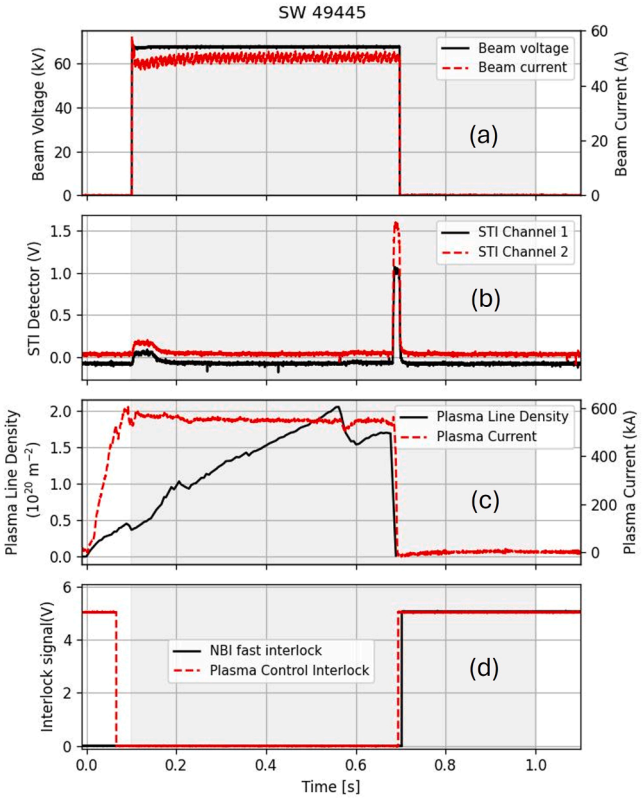

Fig. 16. Operation of the STI on the SW beamline – MAST-U pulse 49445. (a) Beam voltage and current. (b) ST1 output voltages. (c) Plasma line density and plasma current. (c) NBI fast interlock and Plasma Control System voltages. The greyed area shows the preset beam on period (0.9 s).

5.2. *The effect of dust on the beam dump surface*

The shinethrough detector signals shown in Figs. 13, 14 and 15 all show the same notable feature; namely, there is a fast initial rise in the IR signal as the beam is initially turned on followed by a much slower rise in the signal. This behaviour has been observed previously with beam irradiation of graphite surfaces [9]. It has been attributed to micron sized loosely bound material ("dust") on the graphite surface. This dust heats up much faster than the bulk material when the beam is switched on. The contribution of the dust to the STI signal for these beam into vacuum pulses has been investigated using the approach given by Ćirić et al. [9].

The STI signal, V_{tot}, is composed of two parts coming from the dust, V_{dust}, and the bulk material, V_{bulk},

$$V_{tot} = KV_{dust} + (1-K)V_{bulk} \quad (1)$$

where K is the coverage of the dust on the tile. The dust is heated very rapidly, and by assuming that heating and radiation are in equilibrium, its temperature can be estimated by

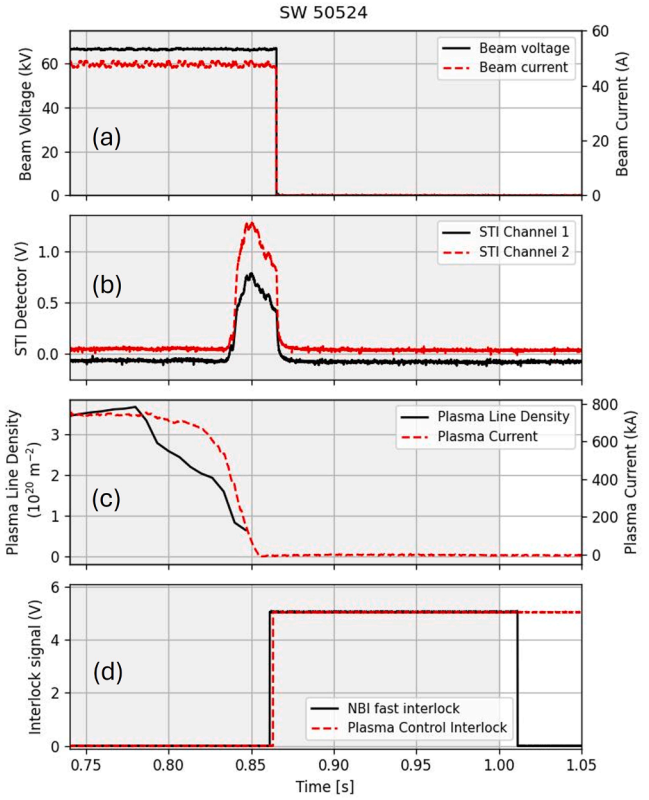

Fig. 17. Operation of the STI on the SW beamline – MAST-U pulse 50524. (a) Beam voltage and current. (b) STI output voltages. (c) Plasma line density and plasma current. (d) NBI fast interlock and Plasma Control System voltages. The greyed area shows the preset beam on period (0.92 s starting at 0.08 s).

$$T_{dust}(^{\circ}C) = \left(\frac{P}{f\sigma}\right)^{1/4} - 273 \tag{2}$$

where P is the incident power density, σ is the Stefan Boltzmann constant and f is the dust form factor. This form factor is related to the shape and orientation of the dust particles with respect to the incident heat flux and is the ratio between the radiative and incident area of the dust particles. For a spherical particle of radius r, $f = 4\pi r^2/\pi r^2 = 4$. For more complicated shapes this value will be higher. The dust emissivity is effectively incorporated into the form factor as they cannot be separated by a fitting procedure.

For the bulk material the temperature rise is given by

$$T_{bulk} = PA\sqrt{t} \tag{3}$$

with t being time and A is a factor related to the material properties which is assumed to be constant with temperature up to temperatures of ~1000 °C [9]. Note that the 1D heat transfer model shown in Fig. 4 is well fitted by this equation. Finally, the measured voltage from these two contributions can be written

$$V_{tot}(V) = aK\left(\left(\frac{P}{f\sigma}\right)^{1/4} - 273\right)^{b} + a(1-K)\left(PA\sqrt{t}\right)^{b} \tag{4}$$

The constants a and b, which relate the temperature to the measured voltage, are determined from a power equation fit to the data in Fig. 11 but with the calibration scaled to the actual gain used of 60 dB. A power fit was used as the data does not quite follow an exponential trend at the highest temperatures measured. Eq. (4) can be fitted, using a least squares routine, to the measured signals to obtain the parameters K, f and A. The incident power density is taken from PINI Simulator. There is a small issue with using this equation in that the emissivity of the dust was assumed to be unity whereas in the calibration of the instrument the emissivity of the tiles was taken as 0.9. However, the emissivity of the dust is effectively incorporated into the form factor f. Also, the a and b constants are derived from a calibration assuming emissivity = 0.9 for the tiles. The difference is likely to be small.

Fig. 18 shows the fit of Eq. (4) to the measured STI signals for SW pulses 48438 and 48444.

The parameters obtained from the fits are given in Table 1. These results give an indication of the effect of the dust on the signals. The coverage is quite low but the dust temperature rise is ~2600–2900 °C. The form factor indicates the dust particles are generally not spherical and maybe even less so if the emissivity is <1. In the higher power pulse (48444) the tile bulk temperature has reached the conservative temperature limit of ~700 °C after the beam duration of 0.14 s.

5.3. Comparison with IR camera measurements

IR cameras (FLIR model AX5) view both the SS and SW beam dumps. The cameras had not been fully calibrated for the emissivity of the beam dump tiles and the correct window transmission and geometry. It was decided to analyse the beam dump heating using the camera for some beam shots. In analysing the images from the camera, the hottest pixel was selected and its indicated temperature was tracked through the pulse. The frames were analysed with assumed emissivities of 0.7 and 0.9, a window transmission of 0.89 and a gap between the window and camera of 0.1 m.

In Fig. 19, the temperature rise determined from the IR camera is shown through the beam into gas pulse 48444 on the SW beamline. Also shown is the bulk temperature rise determined from the analysis of the beam into gas pulses discussed in Section 5.2 and the results of the 1D heat transfer model shown in Fig. 4 using a peak power density of 36 MWm^{-2} obtained from PINI Simulator for the conditions in this pulse.

There is a good agreement between the various sets of data. The temperature determined by the IR images is quite sensitive to the choice of emissivity. The STI data indicates the highest temperatures and thus, derived from an independent analysis, setting the threshold based on it is probably conservative.

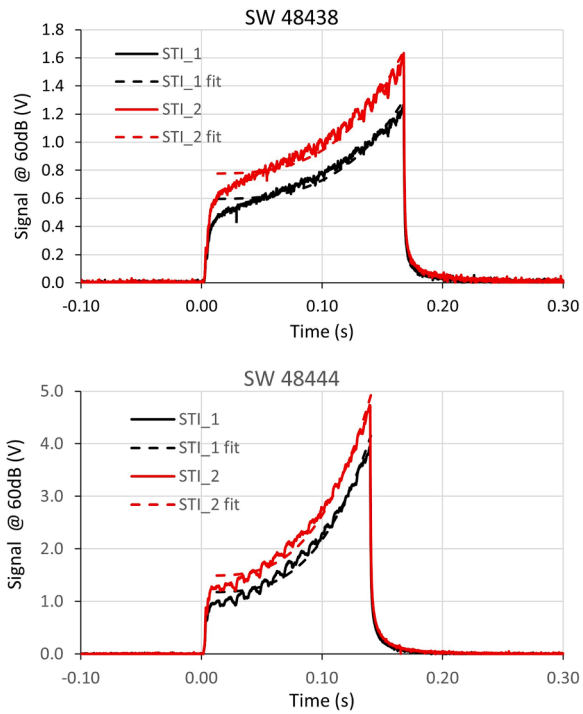

Fig. 18. Fits of Eq. (4) to the STI signals for SW pulses 48438 and 48444.

Table 1
Results of fitting Eq. (4) to the beam into gas STI signals for pulses SW 48438 and SW 48444.

	Pulse			
	SW 48438		SW 48444	
Voltage (kV) and Current (A)	55, 37		65, 48	
Power (MW)	1.18		1.62	
	STI_1	STI_2	STI_1	STI_2
Form factor f	6.75	6.53	6.73	6.54
Coverage K (%)	6.1 × 10^{-3}	7.5 × 10^{-3}	6.3 × 10^{-3}	7.5 × 10^{-3}
Parameter A	56.97	58.91	54.1	55.3
T_{dust} (°C)	2570	2593	2843	2866
T_{bulk} (°C) (end of beam phase)	583	603	727	747

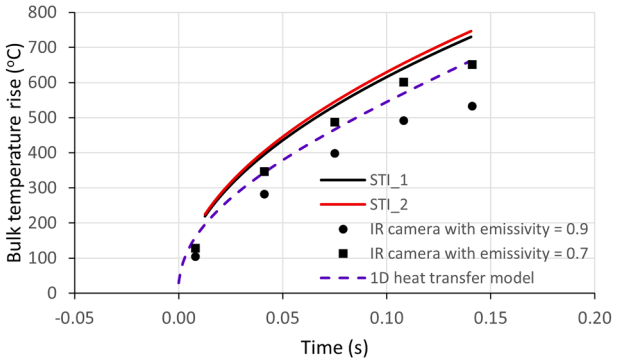

Fig. 19. Comparison of the tile temperature rise during pulse SW 48444 determined from the IR camera for different emssivities, the bulk temperature from the STI detectors and the results of the 1D heat transfer model.

6. Conclusions

A relatively simple shinethrough diagnostic and interlock has been developed to protect the beam dumps for MAST-U NBI operations. The most important part of its setup is the setting of the threshold at which the beam will switch off if the signal exceeds the preset value. If it is set too conservatively then there is the possibility of interrupting the beam operation when not necessary. If set at too high a level, there could be a risk of damage to the beam dumps. Generally, it has been found that setting the threshold at 1 V is compatible with all operating scenarios so far. This voltage corresponds to an estimated bulk temperature rise of ~616 °C based on the analysis presented.

The presence of dust affects the STI signal and the level of dust is likely to be variable. Ćirić et al. [9] concluded that the initial coverage of dust could be reduced by extensive exposure of the tile to high power beams but that even initially clean tiles would develop some dust coverage. Other tokamak components such as the divertor, limiter and coil protection tiles that are made of graphite may also produce dust that is deposited on the beam dump The dust level could change through a pulse. It is not possible to separate the dust and bulk temperature contributions to the signal. The STI signal probably will be always higher than that from that signal originating from the bulk material which is safer from the machine protection point of view.

Future work will attempt to determine the tile emission properties but as mentioned above, this may well be compromised by the level of dust on the tile. The interlock could be made to act even faster by connecting the output signal directly to the high voltage power supplies. This is not possible for the existing supplies but will be under consideration when the power supplies are upgraded.

CRediT authorship contribution statement

Roy McAdams: Writing – original draft, Methodology, Investigation, Conceptualization. **Philippe Jacquet:** Writing – review & editing, Supervision, Methodology, Investigation, Conceptualization. **Ian Day:** Methodology, Investigation. **Effy Rose:** Validation, Methodology, Investigation, Conceptualization. **Andrew Ash:** Investigation. **Jake Ashton:** Investigation. **Hana El-Haroun:** Investigation. **Paul Jepson:** Methodology, Investigation. **David Keeling:** Methodology, Investigation. **Damian King:** Methodology, Conceptualization. **Robert King:** Investigation. **Stephen Marsden:** Software, Investigation. **Alistair McShee:** Investigation. **Maria Nicassio:** Validation, Supervision, Investigation. **Dean Payne:** Investigation. **Robert Proudfoot:** Methodology, Investigation. **Ridhima Sharma:** Investigation. **Jamie Smith:** Software. **Christopher Tame:** Investigation. **Thomas Wilson:** Software, Investigation.

Declaration of competing interest

The authors declare that they have no known competing financial interests or personal relationships that could have appeared to influence the work reported in this paper.

Acknowledgments

This work has been funded by the EPSRC Energy Programme [grant number EP/W006839/1]. To obtain further information on the data and models underlying this paper please contact Publications.Manager@ukaea.uk

For the purpose of open access, the author(s) has applied a Creative Commons Attribution (CC BY) licence (where permitted by UKRI, 'Open Government Licence' or 'Creative Commons Attribution No-derivatives (CC BY-ND) licence' may be stated instead) to any Author Accepted Manuscript version arising.

The authors thank Thorlabs Inc. for permission to use their component drawings.

Data availability

Data will be made available on request.

References

[1] D. Ćirić, et al., Fus. Eng. Des. 86 (2011) 509–512, https://doi.org/10.1016/j.fusengdes.2010.11.035.
[2] D. Stork, et al., Fus. Eng. Des. 47 (1999) 131–172, https://doi.org/10.1016/S0920-3796(99)00081-2.
[3] M.-L. Mayoral, et al., Nucl. Fus. 54 (2014) 033002, https://doi.org/10.1088/0029-5515/54/3/033002.
[4] J.R. Harrison, et al., Nucl. Fusion 64 (2024) 112017, https://doi.org/10.1088/1741-4326/ad6011.
[5] S.J. Gee, et al., Fus. Eng. Des. 74 (2005) 403–407, https://doi.org/10.1016/j.fusengdes.2005.06.094.
[6] F. Dhalla, et al., Fus. Eng. Des. 96-97 (2005) 458–462, https://doi.org/10.1016/j.fusengdes.2015.04.042.
[7] D. Ćirić, et al., in: Proceedings of the 19th IEEE/IPSS Symposium on Fusion Engineering, 2002, pp. 56–59, https://doi.org/10.1109/FUSION.2002.1027641.
[8] Zemax OpticStudio, Ansys, Southpointe 2600 Ansys Drive Canonsburg, PA 15317 USA.
[9] D. Ćirić, et al., in: Proceedings Symposium on Fusion Technology 1994, 1995, pp. 391–394, https://doi.org/10.1016/B978-0-444-82220-8.50066-2.